Wide-range photoabsorption cross-sections of simple metals: large basis-set OPW calculations for sodium

Hikaru Kitamura

Department of Physics, Kyoto University, Sakyo-ku, Kyoto 606-8502, Japan

E-mail: kitamura@scphys.kyoto-u.ac.jp

Abstract.

Photoabsorption cross-sections of simple metals are formulated through a solid-state band theory based on the orthogonalized-plane-wave (OPW) method in Slater's local-exchange approximation, where interband transitions of core and conduction electrons are evaluated up to soft x-ray regime by using large basis sets. The photoabsorption cross-sections of a sodium crystal are computed for a wide photon energy range from 3 to 1800 eV. It is found that numerical results reproduce the existing x-ray databases fairly well for energies above the $L_{2,3}$-edge (31 eV), verifying a consistency between solid-state and atomic models for inner-shell photoabsorption; additional oscillatory structures in the present spectra manifest solid-state effects. Our computed results in the vacuum ultraviolet regime (6-30 eV) are also in better agreement with experimental data compared to earlier theories, although some discrepancies remain in the range 20-30 eV. The influence of the core eigenvalues on the absorption spectra is examined.

PACS numbers: 78.70.Dm, 71.20.-b, 78.20.-e

1. Introduction

Owing to the recent progress in x-ray free-electron lasers (FELs) [1-3], intense coherent x-rays with femtosecond pulse duration are becoming available. When a solid target is irradiated by an x-ray FEL pulse with sufficiently high intensity, many core electrons could be excited resonantly to the conduction band above the Fermi level. A recent vacuum-ultraviolet (VUV) FEL experiment for Sn target [4] has demonstrated ultrafast saturable absorption associated with *N*-shell near-edge excitation. Subsequent theoretical analysis, based on the rate equation combined with the cluster-model electronic-structure calculation, has predicted saturable absorption due to a blue shift of the photoabsorption edge in *K*-shell-excited metallic Li [5]. Broad-band observation of transient photo-response of solids excited by intense x-ray FEL is an outstanding issue in condensed-matter physics, even for the case of simple metals.

Attenuation and scattering of x-rays in *cold* solids have been studied intensively in the past, and have been compiled as databases for the elements throughout the periodic table [6-8]. These databases, however, interpolate various experimental data in separate energy regimes; they also adopt theoretical data for isolated atoms that ignore solid-state effects. Although an atomic model may be appropriate for localized phenomena such as core-electron transitions, its validity should be tested explicitly through solid-state theories. We also note that measurements in the VUV regime may be influenced sensitively by experimental conditions and sample quality. It is thus significant to develop solid-state models that can predict absolute photoabsorption cross-sections over a wide range of photon energies and to compare them with experiments.

A band-theoretic approach to core-level photoabsorption spectra in simple metals was reported earlier by Citrin *et al* [9] based on the empirical pseudopotential method. They analyzed singularities in the spectra near the absorption edge by taking additional account of the many-electron response to the core hole through the Mahan-Nozières-de Dominicis (MND) theory [10]. The effects of electron-core hole interaction on the x-ray absorption near-edge spectra were recently investigated with the linear-response theory based on the time-dependent density-functional theory [11] and with the generalized time-dependent

local-density approximation incorporating dynamical screening [12]; these theories were applied to transition metals rather than to simple metals. On the other hand, evaluation of the spectra far above the edge requires computational cost because the wavefunctions have to be computed up to energies much higher than the Fermi level. Müller *et al* obtained x-ray absorption spectra of 3d and 4d transition metals [13] and palladium [14] for energies up to 200 eV above the edge on the basis of the augmented plane-wave method. More recently, Prange *et al* [15] developed a real-space Green's function formalism that can avoid explicit computations of wave functions; optical constants of Au, Cu, C, etc., were thereby evaluated from optical to hard x-ray regimes.

In this paper, we formulate photoabsorption cross-sections of simple metals with the one-electron band theory by using fairly large orthogonalized-plane-wave (OPW) basis sets [16,17]. We thus compute the absolute cross-sections of metallic Na for a wide photon energy range from 3 eV to 1800 eV. Sodium is a prototypical free-electron-like metal, whose photoabsorption cross-sections (or conductivities) were studied in detail from the infrared to the ultraviolet region near an onset of the interband transition (2 eV) [18,19]. On the other hand, there have been fewer investigations in the VUV regime and they are still controversial. Ching and Callaway [19] performed band-structure calculations of conductivities up to 20 eV, which agree well with the measurements by Sutherland *et al* [20] up to 11 eV but significantly overestimate the experimental data by Sato *et al*. [21] for 13-20 eV. Haensel *et al* [22] measured the shape of photoabsorption spectra from the $L_{2,3}$-edge (31 eV) to 140 eV, but they did not produce absolute cross-sections. The current data on the cross-sections above 50 eV rely largely on atomic calculations [6-8]. In this paper, we shall compare our present calculations with these sets of experimental and theoretical data comprehensively, examining their mutual consistencies.

2. The OPW method

The OPW method, albeit a classic approach to calculate electronic structures of solids [16,17], is suitable for treating electronic transitions from an atomic-like core to plane-wave-like

conduction state in simple metals by keeping their mutual orthogonality. The conduction-electron wave function with wave vector $\boldsymbol{k}$ and band index b is expanded in terms of N_{M} OPW functions as

$$\psi_{\mathbf{k},b}(\mathbf{r}) = \sum_{\mathbf{G}}^{N_{\mathrm{M}}} a_{\mathbf{G}b}(\mathbf{k}) \phi_{\mathbf{k}+\mathbf{G}}^{\mathrm{OPW}}(\mathbf{r}), \tag{1}$$

where $\boldsymbol{G}$ is a reciprocal lattice vector, and

$$\phi_{\mathbf{k}}^{\mathrm{OPW}}(\mathbf{r}) = N_{\mathbf{k}}^{\mathrm{OPW}} \left[\frac{1}{\sqrt{\Omega}} \exp(i\mathbf{k}\bullet\mathbf{r}) - \sum_{c}^{\mathrm{occ}} \sum_{\mu=1}^{N} \langle c\mu | \mathbf{k} \rangle \psi_c(\mathbf{r} - \mathbf{R}_\mu) \right]. \tag{2}$$

Here, Ω denotes the volume of the crystal, $\psi_c(\mathbf{r} - \mathbf{R}_\mu)$ represents the wave function of occupied core orbital c (= 1s, 2s, $2p_x$, etc.), $\boldsymbol{R}_\mu$ is the position of μth nucleus ($\mu = 1, \cdots, N$), $N_{\mathbf{k}}^{\mathrm{OPW}}$ is a normalization constant, and $\langle c\mu | \mathbf{k} \rangle \equiv \int d\mathbf{r}\, \psi_c^*(\mathbf{r} - \mathbf{R}_\mu) \Omega^{-1/2} \exp(i\mathbf{k}\bullet\mathbf{r})$.

The core orbital $\psi_c(\mathbf{r})$ is assumed to be strongly localized at an atomic site and can be approximated by the Hartree-Fock (H-F) wave function for an isolated atom computed by Clementi and Roetti [23]; it is written as a superposition of N_{STO} Slater-type orbitals with quantum numbers $\{n_i, l_i, m_i\}$ as

$$\psi_c(\mathbf{r}) = \sum_{i=1}^{N_{\mathrm{STO}}} c_{ci} \phi_{n_i l_i m_i \zeta_i}(\mathbf{r}), \tag{3}$$

$$\phi_{nlm\zeta}(\mathbf{r}) = \left[\frac{(2\zeta)^{2n+1}}{(2n)!} \right]^{1/2} \frac{1}{a_{\mathrm{B}}^{3/2}} \left(\frac{r}{a_{\mathrm{B}}} \right)^{n-1} \exp\left(-\zeta \frac{r}{a_{\mathrm{B}}} \right) Y_{lm}(\theta, \varphi). \tag{4}$$

Here, a_{B} refers to the Bohr radius, and $Y_{lm}(\theta, \varphi)$ represents the (real) spherical harmonics. We also assume throughout the paper that the core orbitals of neighboring atoms do not overlap; the normalization factor $N_{\mathbf{k}}^{\mathrm{OPW}}$ is then calculated approximately as

$$N_{\mathbf{k}}^{\mathrm{OPW}} \simeq \left[1 - n_{\mathrm{atom}} \Omega \sum_{i,j=1}^{N_{\mathrm{STO}}} \frac{P_{ij}^{\mathrm{core}}}{2} \langle \mathbf{k} | i \rangle \langle j | \mathbf{k} \rangle \right]^{-1/2}, \tag{5}$$

with $\langle j | \mathbf{k} \rangle \equiv \int d\mathbf{r} \phi_{n_j l_j m_j \zeta_j}(\mathbf{r}) \Omega^{-1/2} \exp(i\mathbf{k}\bullet\mathbf{r}) = \langle \mathbf{k} | j \rangle^*$, $P_{ij}^{\mathrm{core}} \equiv 2 \sum_{c}^{\mathrm{occ}} c_{ci} c_{cj}$; and $n_{\mathrm{atom}} (= N / \Omega)$ represents the number density of atoms.

The Schrödinger equation that determines the expansion coefficients $\{a_{\mathbf{G}b}(\mathbf{k})\}$ can

be expressed in the $N_{\mathrm{M}} \times N_{\mathrm{M}}$ matrix form [16],

$$\sum_{\mathbf{G}} H_{\mathbf{G}'\mathbf{G}}(\mathbf{k}) a_{\mathbf{G}b}(\mathbf{k}) = \varepsilon_b(\mathbf{k}) \sum_{\mathbf{G}} S_{\mathbf{G}'\mathbf{G}}(\mathbf{k}) a_{\mathbf{G}b}(\mathbf{k}), \tag{6}$$

where $\varepsilon_b(\mathbf{k})$ $(b = 1, \cdots, N_{\mathrm{M}})$ are the energy eigenvalues, and

$$\begin{aligned} S_{\mathbf{G}'\mathbf{G}}(\mathbf{k}) &= \int d\mathbf{r} \phi^{\mathrm{OPW}*}_{\mathbf{k}+\mathbf{G}'}(\mathbf{r}) \phi^{\mathrm{OPW}}_{\mathbf{k}+\mathbf{G}}(\mathbf{r}) \\ &\simeq N^{\mathrm{OPW}}_{\mathbf{k}+\mathbf{G}'} N^{\mathrm{OPW}}_{\mathbf{k}+\mathbf{G}} \left[\delta_{\mathbf{G}'\mathbf{G}} - n_{\mathrm{atom}} \Omega \sum_{i,j=1}^{N_{\mathrm{STO}}} \frac{P^{\mathrm{core}}_{ij}}{2} \langle \mathbf{k}+\mathbf{G}' | i \rangle \langle j | \mathbf{k}+\mathbf{G} \rangle \right] \end{aligned} \tag{7}$$

is the overlap matrix. The Hamiltonian matrix in equation (6) is evaluated as follows.

$$\begin{aligned} H_{\mathbf{G}'\mathbf{G}}(\mathbf{k}) = N^{\mathrm{OPW}}_{\mathbf{k}+\mathbf{G}'} N^{\mathrm{OPW}}_{\mathbf{k}+\mathbf{G}} \Bigg\{ & \delta_{\mathbf{G}'\mathbf{G}} \frac{\hbar^2 |\mathbf{k}+\mathbf{G}|^2}{2m_e} + n_{\mathrm{atom}} \left[v_{\mathrm{WS}}(\mathbf{G}'-\mathbf{G}) + v_{\mathrm{ex}}(\mathbf{G}'-\mathbf{G}) \right. \\ & \left. - \Omega \sum_{i,j=1}^{N_{\mathrm{STO}}} \sum_{c}^{\mathrm{occ}} \varepsilon_c c_{ci} c_{cj} \langle \mathbf{k}+\mathbf{G}' | i \rangle \langle j | \mathbf{k}+\mathbf{G} \rangle \right] \Bigg\}. \end{aligned} \tag{8}$$

Here, m_{e} refers to the electron mass. The energy eigenvalue ε_c of core state c may be evaluated as $\varepsilon_c \approx -\varepsilon_c^{\mathrm{bind}} + \varepsilon_{\mathrm{F}}$, where $\varepsilon_c^{\mathrm{bind}} (> 0)$ is the experimental binding energy of state c determined through photoelectron measurements of metals [24], and $\varepsilon_{\mathrm{F}} (< 0)$ is the energy at the Fermi level.

In equation (8), $v_{\mathrm{WS}}(q)$ corresponds to the Fourier transform of the electrostatic interaction between a conduction electron and a Wigner-Seitz (WS) sphere,

$$\begin{aligned} v_{\mathrm{WS}}(q) = \frac{4\pi e^2}{q^2} \Bigg\{ & \sum_{i,j} P^{\mathrm{core}}_{ij} \left[F_{is,js}(q) - F_{is,js}(0) \right] - Z \\ & + \frac{3Z}{(qa)^3} \left[\sin(qa) - qa \cos(qa) \right] \Bigg\}, \end{aligned} \tag{9}$$

with $F_{is,js}(q) = \int d\mathbf{r} \phi_{n_i 00 \zeta_i}(\mathbf{r}) \phi_{n_j 00 \zeta_j}(\mathbf{r}) \exp(-i\mathbf{q}\bullet\mathbf{r})$. The WS sphere, with radius $a = (3Z / 4\pi n_{\mathrm{e}})^{1/3}$, consists of an ion core of net charge Ze at the center and uniform conduction electrons of average number density n_{e}. The potential produced by core electrons inside an ion core is accounted for by the term proportional to P^{core}_{ij} in equation (9).

Exchange interactions among electrons are incorporated through the local potential

$v_{\rm ex}(q)$ by Slater [16]. Within the WS approximation, it can be expressed as

$$v_{\rm ex}(q) = -3e^2 \int_{r\le a} d\mathbf{r} \left[\frac{3}{8\pi} n_{\rm e}^{\rm tot}(\mathbf{r}) \right]^{1/3} \exp(-i\mathbf{q}\bullet\mathbf{r}), \tag{10}$$

where the local electron density may be given as

$$n_{\rm e}^{\rm tot}(\mathbf{r}) = \sum_{i,j=1}^{N_{\rm STO}} P_{ij}^{\rm core} \phi_{n_i 00\zeta_i}(\mathbf{r}) \phi_{n_j 00\zeta_j}(\mathbf{r}) + n_{\rm e}. \tag{11}$$

The one-electron potential so constructed assumes uniform distribution of conduction electrons and hence it is not self-consistent. Nevertheless, the resultant band structure can reproduce existing data on sodium fairly well, as we shall show later in section 4.2.

3. Photoabsorption cross-sections

The frequency (ω) dependent photoabsorption cross-section per atom in a solid associated with core-conduction (i.e., bound-free) excitation may be calculated as [5,25]

$$\sigma_{\rm bf}^{\rm abs}(\omega) = \sum_{c}^{\rm occ} \sigma_c^{\rm abs}(\omega), \tag{12a}$$

$$\sigma_c^{\rm abs}(\omega) = 2 \sum_{\mathbf{k}}^{\rm BZ} \sum_{b=1}^{N_{\rm M}} \frac{4\pi^2 e^2}{c\hbar m_{\rm e}^2 \omega} \frac{\left|\mathbf{p}_{\mathbf{k}b,c}\right|^2}{3} \delta\left(\omega - \frac{\varepsilon_b(\mathbf{k}) - \varepsilon_c}{\hbar} \right) (1 - f_{\mathbf{k}b}), \tag{12b}$$

where $\mathbf{p}_{\mathbf{k}b,c} \equiv \int d\mathbf{r}\, \psi_{\mathbf{k}b}^*(\mathbf{r}) (\hbar/i) \nabla \psi_c(\mathbf{r})$ is a dipole transition matrix element, and an average has been taken over the directions of polarization; $f_{\mathbf{k}b}$ is the population of state $\{\boldsymbol{k}b\}$ in the conduction band, which satisfies $f_{\mathbf{k}b} = 0$ for $\varepsilon_b(\mathbf{k}) > \varepsilon_{\rm F}$ and $f_{\mathbf{k}b} = 1$ for $\varepsilon_b(\mathbf{k}) \le \varepsilon_{\rm F}$. The sum over $\mathbf{k}$ is taken in the first Brillouin zone (BZ). With the aid of equations (1) and (3), $\mathbf{p}_{\mathbf{k}b,c}$ can be expressed as

$$\mathbf{p}_{\mathbf{k}b,c} = \sum_{\mathbf{G}}^{N_{\rm M}} a_{\mathbf{G}b}^*(\mathbf{k}) N_{\mathbf{k}+\mathbf{G}}^{\rm OPW} \sum_{i=1}^{N_{\rm STO}} c_{ci} \left[\hbar(\mathbf{k}+\mathbf{G}) \langle \mathbf{k}+\mathbf{G} | i \rangle - \sum_{j,l=1}^{N_{\rm STO}} \frac{P_{jl}^{\rm core}}{2} \langle \mathbf{k}+\mathbf{G} | l \rangle \langle j | \mathbf{p} | i \rangle \right], \tag{13}$$

where $\langle j | \mathbf{p} | i \rangle \equiv \int d\mathbf{r} \phi_{n_j l_j m_j \zeta_j}(\mathbf{r}) (\hbar/i) \nabla \phi_{n_i l_i m_i \zeta_i}(\mathbf{r})$.

The free-free absorption cross-section due to interband transitions of conduction electrons may likewise be written as [25]

$$\sigma_{\mathrm{ff}}^{\mathrm{abs}}(\omega)=\frac{2}{N}\sum_{\mathbf{k}}^{\mathrm{BZ}}\sum_{b,b'=1}^{N_{\mathrm{M}}}\frac{4\pi^2e^2}{c\hbar m_{\mathrm{e}}^2\omega}\frac{\left|\mathbf{p}_{\mathbf{k}b',\mathbf{k}b}\right|^2}{3}\delta\left(\omega-\frac{\varepsilon_{b'}(\mathbf{k})-\varepsilon_b(\mathbf{k})}{\hbar}\right)(f_{\mathbf{k}b}-f_{\mathbf{k}b'}), \tag{14}$$

where

$$\begin{aligned}\mathbf{p}_{\mathbf{k}b',\mathbf{k}b}=&\sum_{\mathbf{G}}^{N_{\mathrm{M}}}a_{\mathbf{G}b'}^{*}(\mathbf{k})a_{\mathbf{G}b}(\mathbf{k})\left|N_{\mathbf{k}+\mathbf{G}}^{\mathrm{OPW}}\right|^2\hbar(\mathbf{k}+\mathbf{G})\\&+n_{\mathrm{atom}}\Omega\sum_{\mathbf{G},\mathbf{G}'}^{N_{\mathrm{M}}}a_{\mathbf{G}'b'}^{*}(\mathbf{k})a_{\mathbf{G}b}(\mathbf{k})N_{\mathbf{k}+\mathbf{G}'}^{\mathrm{OPW}*}N_{\mathbf{k}+\mathbf{G}}^{\mathrm{OPW}}\\&\times\left[-\hbar(2\mathbf{k}+\mathbf{G}+\mathbf{G}')A_{\mathbf{G}'\mathbf{G}}(\mathbf{k})+\mathbf{B}_{\mathbf{G}'\mathbf{G}}(\mathbf{k})\right]\end{aligned} \tag{15}$$

is the matrix element of a vertical transition between two bands b and b', with

$$A_{\mathbf{G}'\mathbf{G}}(\mathbf{k})=\sum_{i,j=1}^{N_{\mathrm{STO}}}\frac{P_{ji}^{\mathrm{core}}}{2}\left\langle\mathbf{k}+\mathbf{G}'\middle|i\right\rangle\left\langle j\middle|\mathbf{k}+\mathbf{G}\right\rangle, \tag{16a}$$

$$\mathbf{B}_{\mathbf{G}'\mathbf{G}}(\mathbf{k})=\sum_{i,j=1}^{N_{\mathrm{STO}}}\sum_{i',j'=1}^{N_{\mathrm{STO}}}\frac{P_{ji}^{\mathrm{core}}}{2}\frac{P_{j'i'}^{\mathrm{core}}}{2}\left\langle\mathbf{k}+\mathbf{G}'\middle|i'\right\rangle\left\langle j'\middle|\mathbf{p}\middle|i\right\rangle\left\langle j\middle|\mathbf{k}+\mathbf{G}\right\rangle. \tag{16b}$$

An advantage of the OPW method is that all the transition matrix elements that enter equations (13) and (15) are expressed in terms of the plane waves and Slater-type orbitals so that they can be evaluated analytically.

Straightforward calculations of equations (12) and (14) yield photoabsorption spectra that oscillate rapidly with energy because of a discontinuous change in one-electron energies and wavefunctions at the Brillouin-zone edge [13,14]. In reality, each excited energy level has a width due to its finite lifetime. The width $\Gamma_{\mathrm{coll}}(E)$ of a state with kinetic energy E in the conduction band may be estimated [13] from the collision mean-free path $\lambda(E)$ according to $\Gamma_{\mathrm{coll}}(E)=\hbar\sqrt{2E/m_{\mathrm{e}}}/\lambda(E)$. For core-level excitation, we additionally take into account the Auger width Γ_c of core state c. These energy widths are incorporated into the bound-free cross-section (12b) through the Lorentzian broadening [13,14], yielding a smoothed cross-section,

$$\overline{\sigma_c^{\mathrm{abs}}}(\omega)=\int_{-\infty}^{\infty}d\omega'\frac{1}{\pi}\frac{\Gamma(\hbar\omega')/2}{(\omega-\omega')^2+\left[\Gamma(\hbar\omega')/2\right]^2}\sigma_c^{\mathrm{abs}}(\omega'), \tag{17}$$

with $\Gamma(\hbar\omega')\equiv\Gamma_{\mathrm{coll}}(\hbar\omega'+\varepsilon_c-\varepsilon_{\mathbf{k}=0})+\Gamma_c$, and $\varepsilon_{\mathbf{k}=0}$ represents the energy at the bottom of the conduction band. The free-free cross-section (14) may likewise be smoothed as

$$\overline{\sigma_{\rm ff}^{\rm abs}}(\omega)=\int_{-\infty}^{\infty}d\omega'\frac{1}{\pi}\frac{\Gamma_{\rm coll}(\hbar\omega')/2}{(\omega-\omega')^2+\left[\Gamma_{\rm coll}(\hbar\omega')/2\right]^2}\sigma_{\rm ff}^{\rm abs}(\omega')\,. \tag{18}$$

The total photoabsorption cross-section is given finally as

$$\sigma_{\rm abs}(\omega)=\sum_{c}^{\rm occ}\overline{\sigma_{c}^{\rm abs}}(\omega)+\overline{\sigma_{\rm ff}^{\rm abs}}(\omega)\,. \tag{19}$$

4. Numerical calculations for sodium

4.1. Computational details

We apply the formalism described in sections 2 and 3 to metallic Na with the body-centered-cubic structure. We adopt Z=1 and $n_{\rm atom}$ = $n_{\rm e}$ = $2.54\times10^{22}\,{\rm cm}^{-3}$, corresponding to a lattice constant of 8.1 a.u. The double-zeta functions [23] ($N_{\rm STO}$ = 12) are employed for the core-electron wavefunctions. The exchange potential (10) is evaluated numerically; the result can be reproduced by the fitting formula,

$$v_{\rm ex}(q)=v_{\rm ex}^{\rm cv}(q)+v_{\rm ex}^{\rm vv}(q)\,, \tag{20}$$

$$v_{\rm ex}^{\rm cv}(q)=-C_1\left(\frac{\pi}{a_1}\right)^{3/2}e^{-(qa_{\rm B})^2/4a_1}-C_2\frac{8\pi a_2}{[(qa_{\rm B})^2+a_2^2]^2}\,, \tag{21a}$$

$$v_{\rm ex}^{\rm vv}(q)=-\frac{6e^2k_{\rm F}}{q^3}\left[\sin(qa)-qa\cos(qa)\right], \tag{21b}$$

with a_1 = 0.933, a_2 = 10.84, C_1 = 2.3, and C_2 = 11.06; $k_{\rm F}=(3\pi^2n_{\rm e})^{1/3}$ refers to the Fermi wavenumber.

In x-ray absorption, the excited electron can enter a conduction band far above the Fermi level, so that the basis set size in equation (1) should be taken sufficiently large compared to the case of VUV absorption. We thus make analyses with two different sets of parameters: $N_{\rm M}$ = 429 is adopted and 1330 k-points are sampled within the 1/48 of the first Brillouin zone for photon energies up to about 50 eV (hereafter referred to as scheme A), whereas $N_{\rm M}$ = 5089 and 165 k-points are sampled for energies beyond about 50 eV (scheme B). The maximum values of G in scheme A and B are $\hbar^2G^2/2m_{\rm e}$ = 0.28 keV and 1.47 keV,

respectively. In both cases, the tetrahedral method [26] is used for the *k*-point sampling.

To solve the secular equation (6), we first orthogonalize the basis sets by diagonalizing the matrix $S_{\mathbf{G}'\mathbf{G}}(\mathbf{k})$, rewriting the equation in the form of an eigenvalue equation [27]. When the basis-set size is large, however, the smallest eigenvalue of $S_{\mathbf{G}'\mathbf{G}}(\mathbf{k})$ may become close to zero (or even negative) due to the linear dependence of OPWs [28], causing numerical errors. To circumvent this problem, we use the canonical orthogonalization scheme [27] and remove one basis function that gives rise to a negative eigenvalue of $S_{\mathbf{G}'\mathbf{G}}(\mathbf{k})$.

The interpolation scheme by Lehmann and Taut [29] has been adopted to carry out the ***k***-integration over the first Brillouin zone in equations (12b) and (14). The collisional width $\Gamma_{\mathrm{coll}}(E)$ has been estimated through the analytic formula for $\lambda(E)$ by Ziaja *et al* [30],

$$\lambda(E) = \frac{\sqrt{E}}{0.02(E-E_{\mathrm{F}})^{1.8}} + \frac{E-0.17}{4.85\ln E - 8.6}, \quad \text{for } E > E_{\mathrm{F}}. \tag{22}$$

Here, $\lambda(E)$ and E are measured in angstrom and eV, respectively; and $E_{\mathrm{F}} = \hbar^2 k_{\mathrm{F}}^2 / 2m_{\mathrm{e}}$ = 3.15 eV is the Fermi energy. The fitting parameters in equation (22) have been determined so as to reproduce the numerical data presented in figure 1 of Ref. [30]. For $E \le E_{\mathrm{F}}$, we set $\Gamma_{\mathrm{coll}}(E)$ =0. We adopt the K-shell Auger width of $\Gamma_{1\mathrm{s}}$ = 0.29 eV estimated by Walters and Bhalla [31] for an isolated Na atom with the Hartree-Fock-Slater approach, and the $L_{2,3}$ Auger width of $\Gamma_{2\mathrm{p}}$ = 0.0015 eV obtained by Almbladh *et al* [32] for metallic Na based on the Green's function method. The L_1-edge is not clearly visible in our computed spectra and hence $\Gamma_{2\mathrm{s}}$ has been neglected.

4.2. Electronic structures

Figure 1 displays the energy band structure computed in scheme A, which is compared with the earlier quantum-defect calculation by Ham [33]. The energy at the conduction-band bottom in the present OPW calculation turns out to be $\varepsilon_{\mathbf{k}=0}$ = −0.246 a.u., while the corresponding value by Ham's calculation [33] is −0.302 a.u. Apart from this constant energy offset, the overall shape of the low-lying energy bands in the present theory turns out to be in good agreement with Ham's result, even though our theory neglects electron

correlation. We remark that our calculation in scheme B gives $\varepsilon_{\mathbf{k}=0} = -0.248$ a.u., which does not differ appreciably from the value in scheme A.

The OPW calculations were also carried out previously by Muda [34]. His one-electron potential takes into account realistic conduction-electron wavefunctions as well as a non-spherical correction to the crystal potential. He thus found that, when the band structure was computed in the local-exchange approximation based on the $X\alpha$ method, the closest agreement with Ham's result was achieved by choosing the α-parameter as unity, which corresponds to Slater's approximation adopted in the present work. The value of $\varepsilon_{\mathbf{k}=0}$ in his calculation is –0.256 a.u, which agrees fairly well with the present result.

In figure 2, we compare our computed band structure (measured from the Fermi level) with the recent first-principles many-body theory by van Schilfgaarde *et al* [35] based on the quasiparticle self-consistent GW (QSGW) scheme. An agreement between the two theories is excellent despite of a considerable difference in the underlying approximations. The present theory also agrees well with the angle-resolved photoemission data by Lyo and Plummer [36], as shown in figure 2.

The density of states (DOS) $\rho(\varepsilon) = (2/N)\sum_{\mathbf{k}}^{\mathrm{BZ}}\sum_{b=1}^{N_{\mathrm{M}}}\delta\left(\varepsilon - \varepsilon_b(\mathbf{k})\right)$ for the conduction band obtained in scheme A is plotted in figure 3. The Fermi level ε_{F} determined through the condition, $\int_{-\infty}^{\varepsilon_{\mathrm{F}}} d\varepsilon\rho(\varepsilon) = Z$, amounts to $\varepsilon_{\mathrm{F}} = -3.61$ eV. The computed DOS fluctuates around the free-electron value $\rho(\varepsilon) = 3\left(\varepsilon - \varepsilon_{\mathbf{k}=0}\right)^{1/2} / 2E_{\mathrm{F}}^{3/2}$, exhibiting nonsmooth structures above ε_{F}. We find in figure 3 that the DOS in this work agrees fairly well with that obtained recently by Huotari *et al* [37] with the density-functional theory in the local-density approximation (LDA). In figure 4, logarithmic plot of the DOS is shown for energies up to 1 keV. Here, numerical results in scheme A for $\varepsilon < 50$ eV and those in scheme B for $\varepsilon > 50$ eV are matched at $\varepsilon = 50$ eV. We observe that the DOS eventually merges into the free-electron result for high energies. This does not mean, however, that the free-electron approximation applies for photoabsorption cross-sections, as we shall demonstrate in section 4.3.

4.3. Photoabsorption cross-sections

The photoabsorption cross-section obtained through equation (19) is indicated in figure 5 and compared with various theories and experiments. We first remark that experimental papers often publish the values of the real part of the conductivity $\mathrm{Re}\,\sigma(\omega)$, the imaginary part of the dielectric constant $\mathrm{Im}\,\varepsilon(\omega)$, or the absorption coefficient $\kappa_{\mathrm{abs}}(\omega)$, instead of the photoabsorption cross-section; these quantities are related to each other via the relation,

$$\sigma_{\mathrm{abs}}(\omega) = \frac{4\pi}{n_{\mathrm{atom}}c}\mathrm{Re}\,\sigma(\omega) = \frac{\omega}{n_{\mathrm{atom}}c}\mathrm{Im}\,\varepsilon(\omega) = \frac{n(\omega)}{n_{\mathrm{atom}}}\kappa_{\mathrm{abs}}(\omega),$$

where $n(\omega)$ is a real part of the refractive index, which is close to unity for energies greater than about 20 eV in the case of Na [8,21].

Inagaki *et al* [18] measured the conductivities of evaporated Na films at room temperature for $\hbar\omega = 0.6$-3.8 eV by means of ellipsometry. It can be seen that the present work underestimates the photoabsorption especially near an onset of interband transition at 2 eV. Validity of the present theory may not be ensured for energies below approximately 3 eV, because the electron-phonon scattering [25] neglected in this paper plays an important role at such low energies [19].

In the energy range from 6 to 11 eV, where the photoabsorption occurs through interband transitions within the conduction band, the prediction of our OPW calculation is in good agreement with the measurements by Sutherland *et al* [20] (filled circles) for evaporated Na films. At higher energies, our computed photoabsorption cross-sections *decrease* gradually toward the $L_{2,3}$-edge, while the measurements of Sato *et al* [21] (crosses) exhibit a gradual *increase* from 15 to 26 eV. Thus, a relatively large discrepancy between these two sets of results can be seen in the range 20-30 eV.

Theoretical calculation of conductivities in this energy range was performed previously by Ching and Callaway [19] on the basis of the self-consistent linear-combination-of-atomic-orbitals (LCAO) band calculations using Gaussian-type orbitals. Their conductivities are in good accord with the measurements by Sutherland *et al* [18] below 11 eV, whereas they increase drastically above 13 eV, showing prominent peaks at about 16 eV and 19 eV; Sato *et al* [21] did not detect such peaks, and their measured conductivities

were smaller by more than one order of magnitude. Sato *et al*'s data [21] are thus in closer agreement with the present work than with Ching-Callaway theory [19].

At still higher energies, the absorption spectra are dominated by inner-shell excitations, characterized by the $L_{2,3}$-edge at 31 eV, L_1-edge at 63 eV, and *K*-edge at 1071 eV [6-8]. As indicated in figure 5, our cross-sections below 50 eV obtained in scheme A can be joined smoothly into those above 50 eV obtained in scheme B, indicating an internal consistency. It is remarkable that the present theory exhibits overall agreement with the NIST database by Chantler [6] (chain line) and the database by Henke *et al* [7] (triangles) over a wide energy range up to 1800 eV, although these databases are based on atomic theories.

For comparison, we plot in figure 5 the numerical results of the 1-OPW approximation, in which equation (1) is approximated by a single OPW, $\psi_{\mathbf{k}}(\mathbf{r}) = \phi_{\mathbf{k}}^{\mathrm{OPW}}(\mathbf{r})$, with the one-electron energy $\varepsilon_{\mathbf{k}} = \hbar^2 k^2 / 2m_{\mathrm{e}}$ in the free-electron approximation. The bound-free photoabsorption cross-section is calculated with equation (12b) where the summation over *b* is omitted and the summation over $\boldsymbol{k}$ runs over the entire *k*-space (i.e., extended-zone scheme). It can be clearly seen that such a 1-OPW calculation fails to reproduce the existing databases even for energies away from the absorption edges.

Figure 6 exhibits magnified spectra in the energy range from 20 to 150 eV. The NIST cross-section varies smoothly with energy, whereas the present spectrum exhibits oscillatory structures stemming from solid-state effects. We also plot in figure 6 the absorption spectrum measured by Haensel *et al* [22] in arbitrary units, which exhibits three broad peaks at 48.5 eV, 65.5 eV and about 90 eV. It is notable that the present theory also predicts these peaks, although our central peak is considerably higher than the other two in contrast to the experimental data [22]. The sharp peaks at the onset of the L_2- and L_3-edges were previously attributed [9,10,22] to the spin-orbit splitting and the threshold singularities of MND type, which are both neglected in the present theory. The absorption by 2s-electrons sets in at 63 eV, but their contribution to the total cross-section is small and hence the L_1-edge is not prominent.

The absorption spectra above the *K*-edge are indicated in figure 7. The present OPW cross-section exhibits oscillations arising from solid-state effects, while its overall

behavior agrees fairly well with the x-ray databases [6,7]. The 1-OPW approximation, however, deviates considerably from these databases, predicting a spurious local minimum at about 1.3 keV. Such a failure of the 1-OPW approximation was pointed out by Williams and Shirley [38] in connection with the *K*-shell photoionization of a neon atom. They showed that the spurious minimum disappears when the final-state wavefunction is calculated accurately through numerical integrations of the Schrödinger equation. Similarly, we observe in figure 7 that the full band theory significantly improves the 1-OPW result, which implies that a superposition of a sufficiently large number of OPW functions leads to an accurate description of final-state wavefunctions in solids.

Finally, we mention how the assessments of the core energy eigenvalues affect the resultant photoabsorption cross-sections. The parameter values of ε_{1s}, ε_{2s} and ε_{2p} employed in this work are −1075, −67 and −35.2 eV, respectively, which are based on photoelectron measurements [24]. The corresponding values in the atomic H-F theory [23] are −1101, −76 and −41.2 eV, respectively. Figure 8 compares the photoabsorption cross-sections obtained by using these two sets of core energies. We find that, in the H-F case, the $L_{2,3}$-edge energy is overestimated by about 6 eV, and that the use of the experimental core levels [24] can achieve closer agreement with experimental cross-sections as a whole [7,21]. We remark that ε_c not only controls the absorption cross-section directly through equation (12b) but enters the Hamiltonian matrix element (8), which in turn modifies the cross-sections indirectly. In passing, the corresponding core eigenvalues in LDA, which are available through the Atomic Reference Data for Electronic Structure Calculations produced by NIST database [39], are −1026, −56.1 and −28.9 eV, respectively. Hence, the core eigenvalues employed in the present work lie between the H-F and LDA values.

5. Concluding remarks

We have formulated the photoabsorption cross-sections of simple metals through the one-electron band theory by combining large OPW basis sets for conduction electrons, H-F atomic wavefunctions for core electrons, and experimental binding energies for core

eigenvalues. Broad-range photobsorption cross-sections of Na metal for photon energies of 3-1800 eV have been computed for the first time, and they have been compared with earlier theories, experiments, and x-ray databases. We have thus confirmed that the inner-shell photoabsorption cross-sections computed by the present theory are consistent with the x-ray databases based on atomic theories. Our absorption cross-sections in the VUV regime associated with interband excitation of conduction electrons also reproduce the available experimental data fairly well. The present theory cannot account for the gradual increase of absorption from 15 to 26 eV measured by Sato *et al* [21], but significantly improves an earlier theory in this energy range.

In the present OPW approach, the matrix elements of radiative transitions can be evaluated analytically since they are expressed in terms of the plane waves and Slater-type functions. Similarly, analytical calculations of two-electron Coulomb repulsion integrals [5] would enable one to incorporate screening of the laser field, electron-hole and electron-electron correlations. Thus, the simplicity of the OPW formalism may be advantageous for developing advanced theoretical tools to analyze complicated interactions between metallic electrons and intense x-ray FELs.

Acknowledgments

The author is grateful to Dr S Huotari for providing the numerical data on the density of states in Ref [37]. The author also wishes to thank Dr H Yoneda for pertinent discussions and Dr B Ziaja for correspondence. This work was supported in part through Grant-in-Aid for Young Scientists (B) provided by the Japanese Ministry of Education, Culture, Sports, Science and Technology (MEXT).

References

[1] Yabashi M and Ishikawa T eds 2010 XFEL/SPring-8 Beamline Technical Design Report Ver. 2.0, RIKEN/JASRI

[2] Arthur J *et al* 2002 Linac Coherent Light Source (LCLS) Conceptual Design Report, SLAC-R593, Stanford

[3] Altarelli M *et al* eds 2007 The European X-Ray Free-Electron Laser Technical Design Report, DESY 2006-097

[4] Yoneda H *et al* 2009 *Opt. Express* **17** 23443

[5] Kitamura H 2010 *J. Phys. B: At. Mol. Opt. Phys.* **43** 115601

Kitamura H 2012 *High Ene. Dens. Phys.* **8** 66

[6] Chantler C T 1995 *J. Phys. Chem. Ref. Data* **24** 71

[7] Henke B L, Gullikson E M and Davis J C 1993 *At. Data Nucl. Data Tables* **54** 181

[8] Lynch D W and Hunter W R 1991 *Handbook of optical constants of solids* II, ed E.D. Palik (California: Academic Press) p 341

[9] Citrin P H, Wertheim G K and Schlüter M 1979 *Phys. Rev.* B **20** 3067

[10] Mahan G D 1974 *Sol. State. Phys.* **29**, ed. H. Ehrenreich, F.Seitz and D. Turnbull p 75

[11] Schwitalla J and Ebert H 1998 *Phys. Rev. Lett.* **80** 4586

[12] Ankudinov A L, Nesvizhskii A I and Rehr J J 2003 *Phys. Rev.* B **67** 115120

[13] Müller J E, Jepsen O and Wilkins J W 1982 *Sol. State Comm.* **42** 365

[14] Müller J E and Wilkins J W 1984 *Phys. Rev.* B **29** 4331

[15] Prange M P, Rehr J J, Rivas G, Kas J J and Lawson J W 2009 *Phys. Rev.* B **80** 155110

[16] Woodruff T O 1957 *Sol. State Phys.* **4** 367

[17] Harrison W A 2005 *Elementary Electronic Structure* (Singapore: World Scientific) chap 15

[18] Inagaki T, Emerson L C, Arakawa E T and Williams M W 1976 *Phys. Rev.* B **13** 2305

[19] Ching W Y and Callaway J 1975 *Phys. Rev.* B **11** 1324

[20] Sutherland J C, Hamm R N and Arakawa E T 1969 *J. Opt. Soc. Am.* **59** 1581

[21] Sato S, Miyahara T, Hanyu T, Yamaguchi S and Ishii T 1979 *J. Phys. Soc. Jpn.* **47** 836

[22] Haensel R, Keitel G, Sonntag B, Kunz C and Schereiber P 1970 *Phys. Stat. Sol.* (a)**2** 85

[23] Clementi E and Roetti C 1974 *At. Data Nucl. Data Tables* **14** 177

[24] Fuggle J C and Mårtensson N 1980 *J. Elec. Spec. Rel. Phenom.* **21** 275

[25] Bassani F and Altarelli M 1983 *Handbook of Synchrotron Radiation*, vol 1, ed E E Koch (Amsterdam: North-Holland) p 463

[26] Zaharioudakis D 2004 *Comp. Phys. Comm.* **157** 17

[27] Szabo A and Ostlund N S 1982 *Modern Quantum Chemistry: Introduction to Advanced Electronic Structure Theory* (New York: Macmillan) sec 3.4.5

[28] Girardeau M D 1971 *J. Math. Phys.* **12** 165

[29] Lehmann G and Taut M 1972 *Phys. Stat. Sol.* (b) **54**, 469

[30] Ziaja B, London R A and Hajdu J 2006 *J. Appl. Phys.* **99** 033514

[31] Walters D L and Bhalla C P 1971 *Atomic Data* **3** 301

[32] Almbladh C -O, Morale A L, Grossmann G 1989 *Phys. Rev.* B **39** 3489

[33] Ham F S 1962 *Phys. Rev.* **128** 82

[34] Muda Y 1971 *J. Phys. Soc. Jpn.* **31** 1329

[35] van Schilfgaarde M, Kotani T and Faleev S 2006 *Phys. Rev. Lett.* **96** 226402

[36] Lyo I-W and Plummer E W 1998 *Phys. Rev. Lett.* **60** 1558

[37] Huotari S, Cazzaniga M, Weissker H –C, Pylkkänen T, Müller H, Reining L, Onida G and Monaco G 2011 *Phys. Rev.* B **84** 075108

[38] Williams R S and Shirley D A 1977 *J. Chem. Phys.* **66** 2378

[39] Kotochigova S, Levine Z H, Shirley E L, Stiles M D and Clark C W 1997 *Phys. Rev.* A **55** 191

Figure captions

Figure 1. Conduction-band structures for solid Na. The filled circles depict numerical solutions to equation (6), with ε_F indicating the Fermi level; the dotted curves with crosses are the results of Ham [33].

Figure 2. Comparison of the conduction-band structures for solid Na obtained by the present work (solid curves), QSGW theory [35] (squares), and photoemission data [36] (empty circles).

Figure 3. The density of states for solid Na near the Fermi level. The solid curve is the present result; the dashed curve corresponds to the free-electron approximation; the dotted curve represents the LDA calculation [37] where the position of the conduction-band bottom has been adjusted to the present data.

Figure 4. The density of states for solid Na on a logarithmic scale.

Figure 5. Photoabsorption cross-sections for solid Na.

Figure 6. Photoabsorption cross-sections for solid Na near and above the $L_{2,3}$-edge. The dashed curve depicts the contribution of $\overline{\sigma_{2s}^{\mathrm{abs}}}(\omega)$. The experimental data by Haensel *et al* [22] are plotted in arbitrary units and scaled by the right axis.

Figure 7. Photoabsorption cross-sections for solid Na near and above the *K*-edge. The solid curve is the result from equation (19); the dotted curve is the corresponding result without Lorentzian broadening.

Figure 8. Photoabsorption cross-sections for solid Na obtained through two different assessments of ε_c. The solid and dashed curves adopt experimental core levels of Na metal

[24] and H-F energy levels of an isolated Na atom [23], respectively.

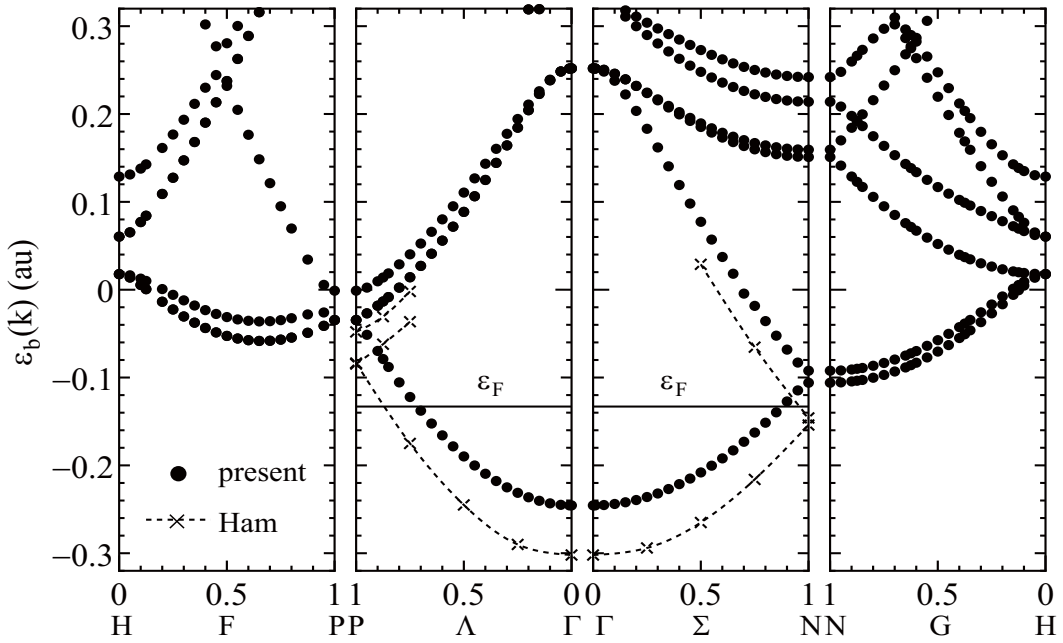
0.3
0.2
0.1
0
−0.1
−0.2
−0.3
$\varepsilon_b(k)$ (au)
present
Ham
ε_F
ε_F
0
0.5
1
H
F
P
Λ
Γ
Σ
N
G
H

Figure 1

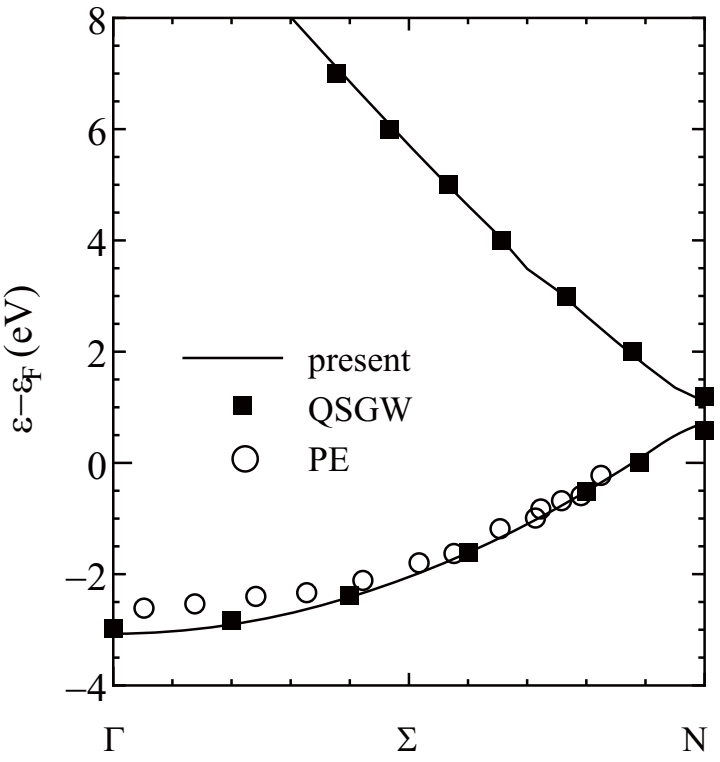

Figure 2

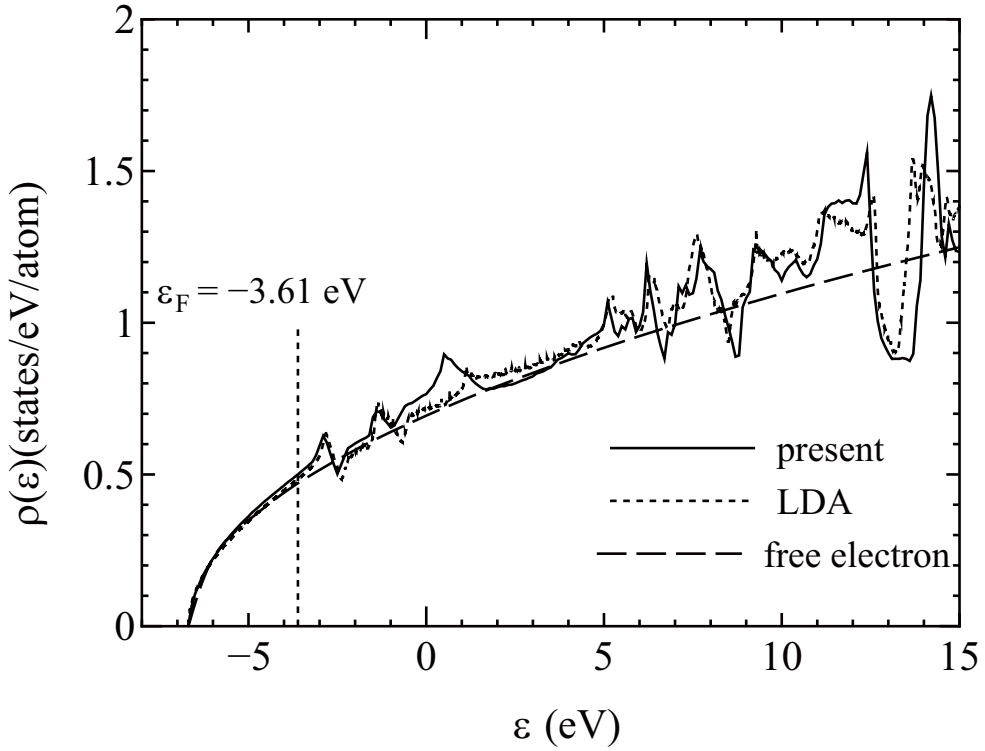
2
1.5
1
0.5
0
ρ(ε)(states/eV/atom)
εF = −3.61 eV
present
LDA
free electron
−5
0
5
10
15
ε (eV)

Figure 3

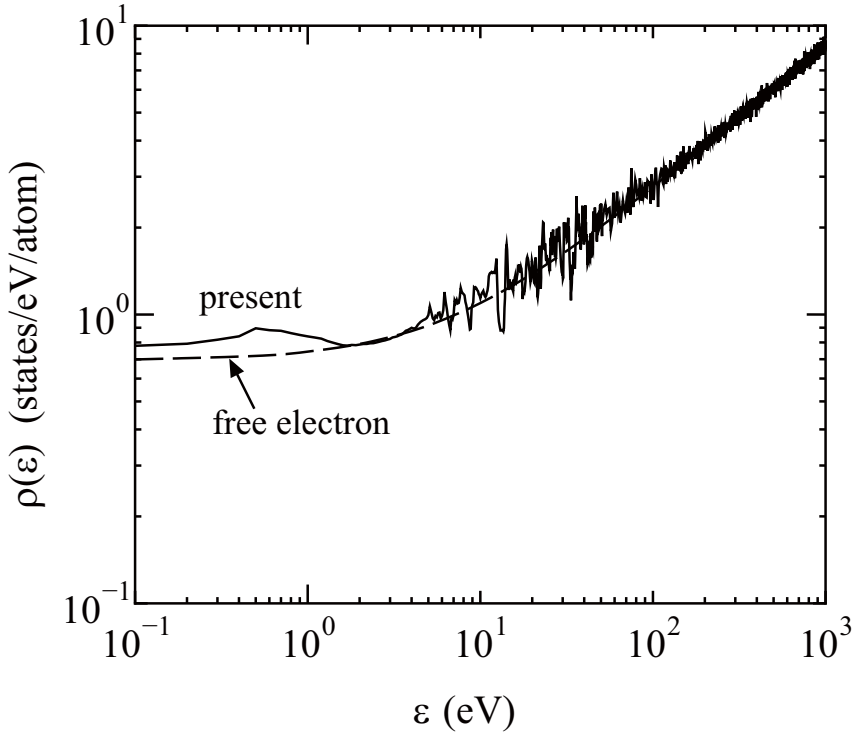
10^1
10^0
10^{-1}
10^{-1}
10^0
10^1
10^2
10^3
ρ(ε) (states/eV/atom)
ε (eV)
present
free electron

Figure 4

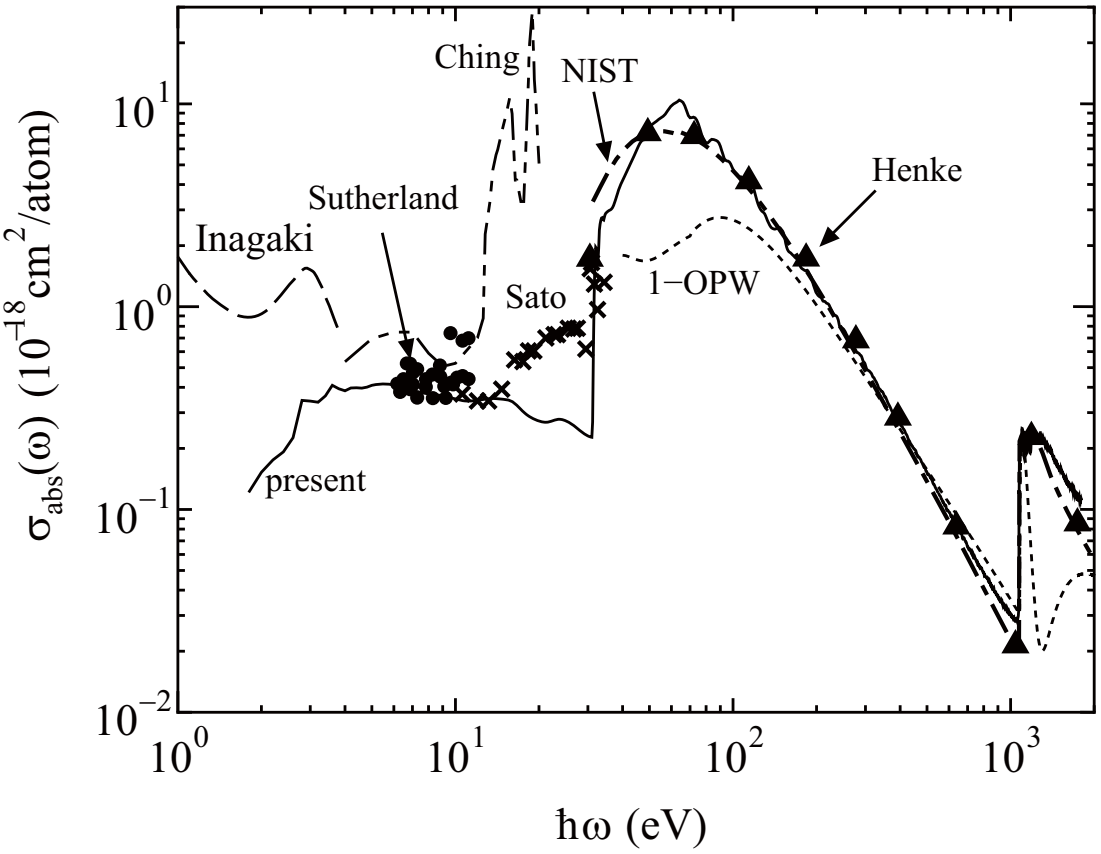
Ching
NIST
Henke
Sutherland
Inagaki
Sato
1−OPW
present
$\sigma_{abs}(\omega)$ (10^{-18}cm^2/atom)
$\hbar\omega$ (eV)

Figure 5

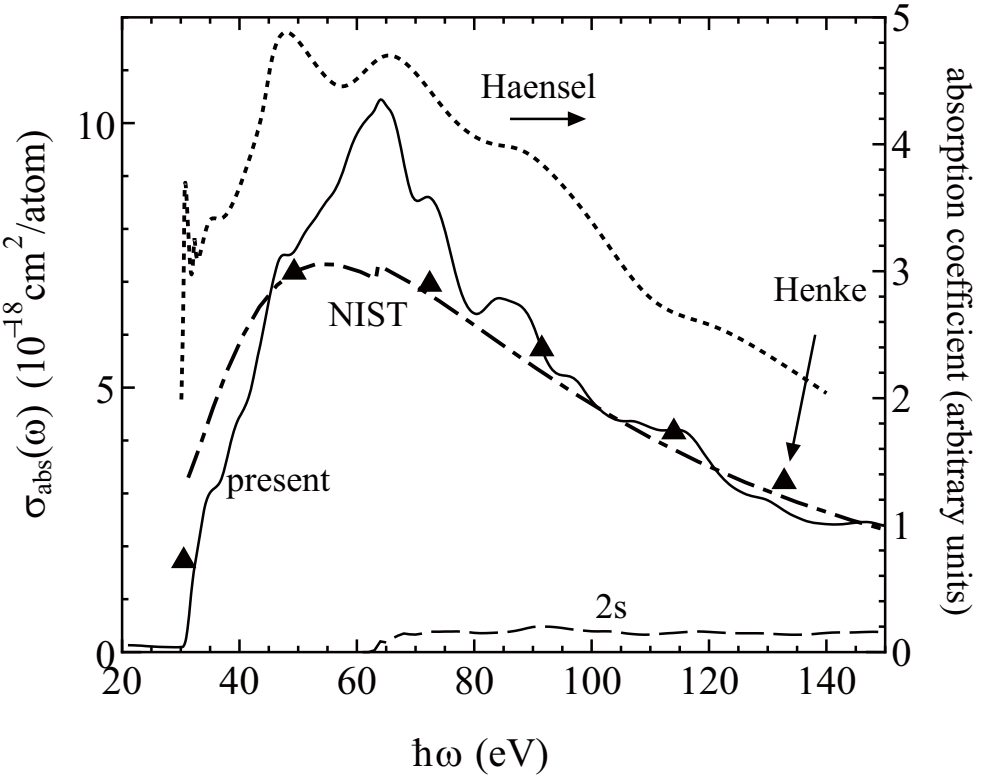
Haensel
Henke
NIST
present
2s
$\sigma_{abs}(\omega)$ (10^{-18}cm^2/atom)
absorption coefficient (arbitrary units)
ħω (eV)
0
5
10
0
1
2
3
4
5
20
40
60
80
100
120
140

Figure 6

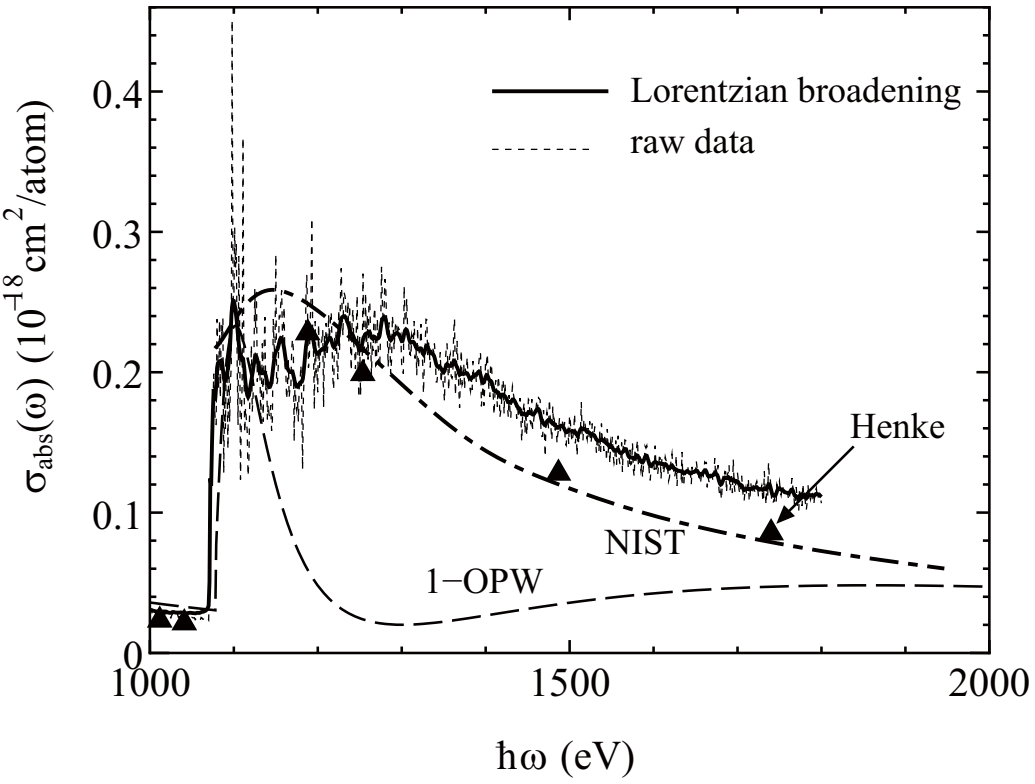
Lorentzian broadening
raw data
Henke
NIST
1−OPW
0.4
0.3
0.2
0.1
0
1000
1500
2000
ħω (eV)
σabs(ω) (10−18cm2/atom)

Figure 7

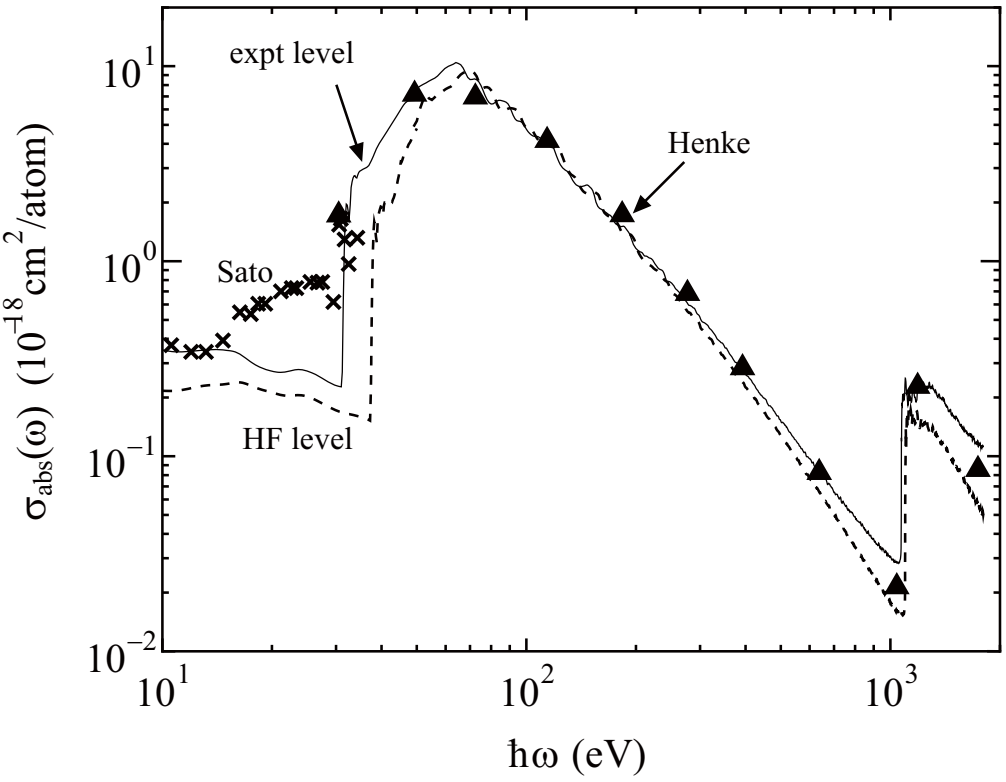
expt level
Henke
Sato
HF level
$\sigma_{abs}(\omega)$ $(10^{-18}\text{cm}^2/\text{atom})$
$\hbar\omega$ (eV)
10^{1}
10^{0}
10^{-1}
10^{-2}
10^{1}
10^{2}
10^{3}

Figure 8